Kelvin Waves and Tropical Cyclogenesis: A Global Survey

CARL J. SCHRECK III

North Carolina Institute for Climate Studies, North Carolina State University, Asheville, North Carolina

(Manuscript received 23 March 2015, in final form 11 June 2015)

ABSTRACT

Convectively coupled atmospheric Kelvin waves are among the most prominent sources of synoptic-scale rainfall variability in the tropics, but large uncertainties surround their role in tropical cyclogenesis. This study identifies the modulation of tropical cyclones relative to the passage of a Kelvin wave's peak rainfall (i.e., its crest) in each basin. Tropical cyclogenesis is generally inhibited for 3 days before the crest and enhanced for 3 days afterward. Composites of storms forming in the most favorable lags illustrate the dynamical impacts of the waves. In most basins, the tropical cyclone actually forms during the convectively suppressed phase of the wave. The 850-hPa equatorial westerly anomalies provide the cyclonic vorticity for the nascent storm, and 200-hPa easterly anomalies enhance the outflow. The wind anomalies persist at both levels longer than the Kelvin wave's period and are often related to the Madden–Julian oscillation (MJO). The onset of these wind anomalies occurs with the Kelvin wave passage, while the MJO apparently establishes their duration. Many of the composites also show evidence of an easterly wave from which the tropical cyclone develops. The composite easterly wave amplifies or even initiates within the Kelvin wave crest. These results show the importance of Kelvin waves interacting with the MJO and easterly waves during tropical cyclogenesis. Given that Kelvin waves often circumnavigate the globe, these results show promise for long-range forecasting of tropical cyclogenesis in all basins.

1. Introduction

Kelvin waves represent a prominent mode of synoptic-scale (3–10 day) variability within the tropics (Kiladis et al. 2009). More spectral power is associated with these waves than with easterly waves (Wheeler and Kiladis 1999; Roundy and Frank 2004), yet Kelvin waves have received much less attention with regard to tropical cyclogenesis. This study will fill that gap by exploring the relationship between Kelvin waves and tropical cyclogenesis around the globe.

Convectively coupled Kelvin waves have propagation characteristics and horizontal structures that are consistent with linear shallow-water solutions (Takayabu and Murakami 1991; Straub and Kiladis 2003a). They typically move eastward with phase speeds of 10–20 m s^{-1} and wavelengths of 3000–7000 km (Wheeler and Kiladis 1999; Roundy 2008). Developing tropical cyclones usually move the opposite direction, westward, so their intersection with Kelvin waves may be fairly brief. Even so, Kelvin waves can trigger cyclogenesis within other systems like easterly waves (Ventrice et al. 2012a), the Madden–Julian oscillation (MJO; Schreck and Molinari 2011), or the monsoon trough (Frank and Roundy 2006).

No consensus has been found regarding the role of Kelvin waves in tropical cyclone activity. Sobel and Camargo (2005) showed evidence of an inverse relationship in which tropical cyclones can actually spawn Kelvin waves. Frank and Roundy (2006) observed that Kelvin waves play at most a minor role in cyclogenesis compared with other equatorial wave types. Bessafi and Wheeler (2006) found only a small, though statistically significant, modulation of tropical cyclogenesis by Kelvin waves. Kelvin waves have also been found to enhance easterly wave activity over Africa (Mekonnen et al. 2008; Ventrice and Thorncroft 2013), which could increase cyclogenesis over the Atlantic. However, that connection has not been fully explored.

Schreck et al. (2011, 2012) examined the role of equatorial waves in enhancing deep convection for tropical cyclogenesis. They filtered NASA Tropical Rainfall Measuring Mission (TRMM) Multisatellite Precipitation Analyses (TMPA, TRMM product 3b42; Huffman et al. 2007) for each equatorial wave type following Kiladis et al. (2005, 2009). Tropical cyclogenesis

Corresponding author address: Carl J. Schreck III, North Carolina Institute for Climate Studies, 151 Patton Ave., Asheville, NC 28801.
E-mail: cjschrec@ncsu.edu

DOI: 10.1175/MWR-D-15-0111.1

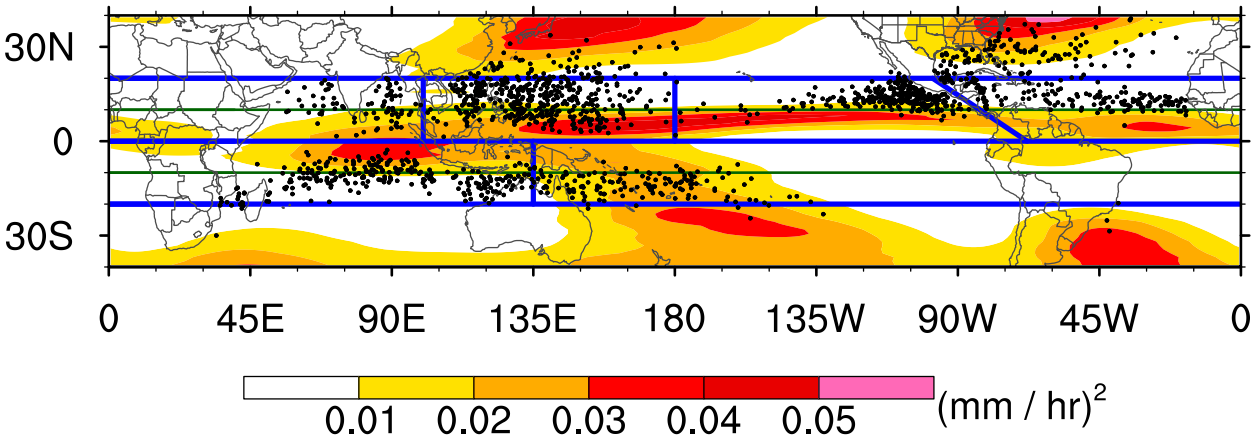

FIG. 1. Variance of Kelvin-filtered rainfall (shading) overlaid with tropical cyclogenesis locations during 1998–2013. Basins used in this study are outlined in blue, whereas green lines at 10°N and 10°S indicate the latitude bands used for identifying the Kelvin waves.

was attributed to a given wave's convection if its filtered rainfall anomaly exceeded a threshold value at the genesis location. This method attributed a comparable number of western Pacific tropical cyclone formations to Kelvin waves as to mixed Rossby–gravity or equatorial Rossby waves. Over the north Indian Ocean, up to 35% of tropical cyclone formations were attributed to Kelvin waves. Schreck et al. (2011, 2012) only considered the role of Kelvin waves in enhancing convection. Recent studies (Schreck and Molinari 2011; Ventrice et al. 2012a,b) have demonstrated that Kelvin waves also influence cyclogenesis by modulating potential vorticity, vertical wind shear, and total column water vapor.

Schreck and Molinari (2011) examined the development of Typhoons Rammasun and Chataan over the western North Pacific in 2002. They identified a series of three Kelvin waves that were embedded within the MJO's convective envelope. With the passage of each Kelvin wave, trade easterlies progressively gave way to equatorial westerlies. These westerlies provided a strip of cyclonic vorticity that broke down into the tropical cyclone vortices in the wake of the third Kelvin wave.

Ventrice et al. (2012a) examined the role of a Kelvin wave in the formation of Tropical Storm Debby (2006) during the NASA African Monsoon Multidisciplinary Analyses (NAMMA). Tropical cyclogenesis occurred when the Kelvin wave combined with the diurnal cycle to enhance a fledgling easterly wave's convection. They also showed climatologically that more tropical cyclones formed in the Atlantic main development region (MDR) after the passage of a Kelvin wave than before. Ventrice et al. (2012b) attributed the variations in tropical cyclone activity to the modulation of vertical wind shear and low-level vorticity by the Kelvin waves.

Together, these studies illustrate the need for a census of the dynamical impacts of Kelvin waves on tropical cyclogenesis around the globe. This study addresses that need by examining the frequency of tropical cyclogenesis on each day before and after the passage of a Kelvin wave's peak rainfall (i.e., the wave *crest*). Composites of storms forming in the most favorable phases of the waves will then illustrate the dynamical effects of Kelvin waves on tropical cyclogenesis in each basin.

2. Data and methods

a. Data

Tropical cyclogenesis in this study is defined as the first location in the best track data from NOAA's National Hurricane Center (NHC) or the Joint Typhoon Warning Center (JTWC), as obtained from the International Best Track Archive for Climate Stewardship (IBTrACS) (Knapp et al. 2010; Schreck et al. 2014). The convective anomalies associated with the Kelvin waves and the MJO are identified using NASA's TMPA (Huffman et al. 2007). The dynamical fields associated with the waves are identified using NASA's Modern-Era Retrospective Analysis for Research and Applications (MERRA; Rienecker et al. 2011). The rainfall estimates were averaged from their native resolution of 0.25°, 3-hourly grids to 1.25°, 6-hourly grids for computational efficiency, and to match the resolution of the MERRA data.

These rainfall estimates are filtered in zonal wavenumber and frequency following previous studies by Kiladis et al. (Wheeler and Kiladis 1999; Straub and Kiladis 2002; Kiladis et al. 2005). The Kelvin wave filter is bounded by eastward-propagating zonal wavenumbers 1–14, periods of 2–17 days, and the shallow-water dispersion curves for equivalent depths of 8 and 90 m (Straub and Kiladis 2002). The MJO filter includes eastward-propagating wavenumbers 0–9, including the zonal mean, and periods of 30–96 days

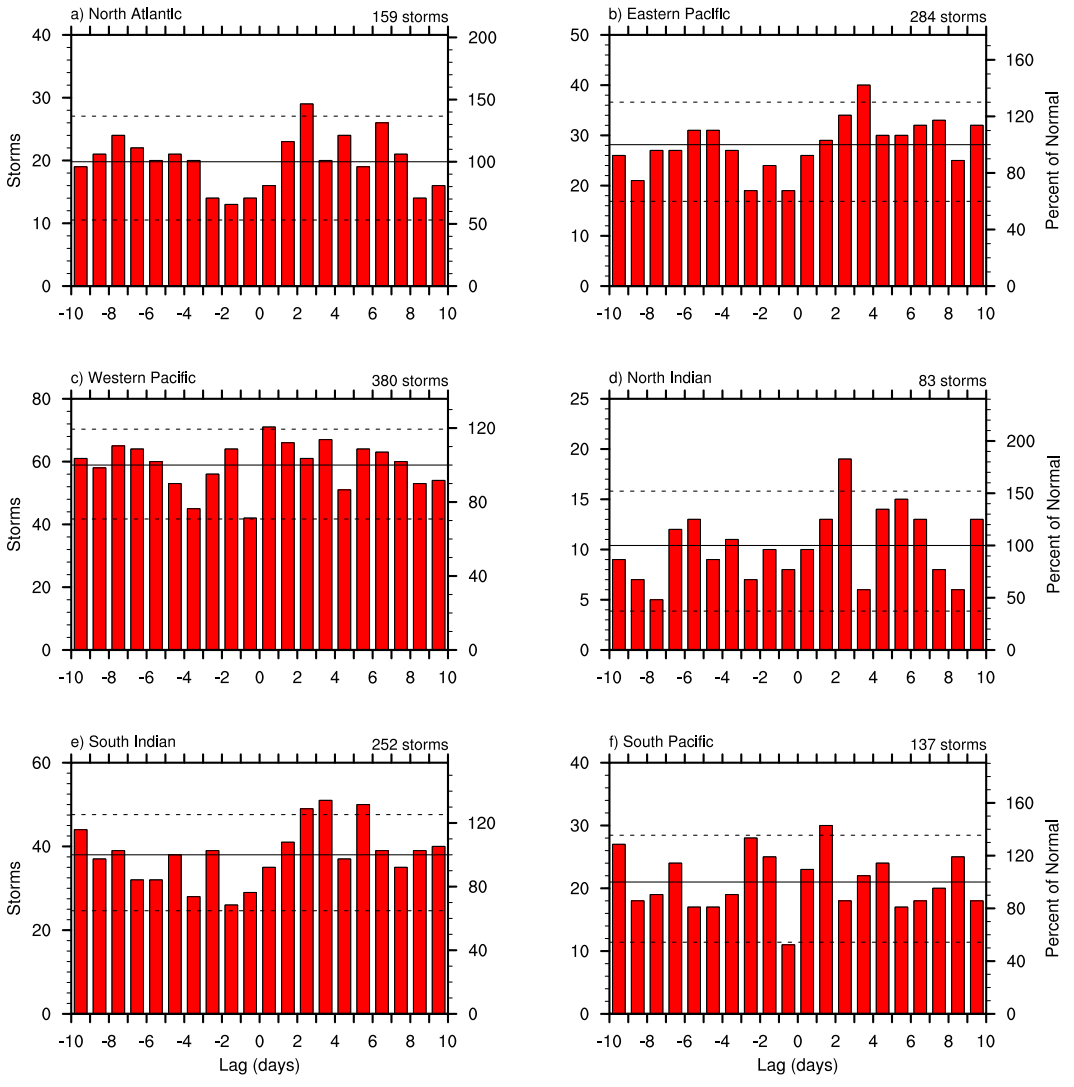

FIG. 2. Histograms of tropical cyclogenesis by lag relative to Kelvin wave crests for each basin. Positive lags indicate that the wave crest preceded cyclogenesis. Solid horizontal lines denote the mean for all lags, while dashed lines identify the 95% probability range. Numbers in the top right indicate the number of storms analyzed in each basin. Storms are counted relative to all Kelvin wave crests not just the nearest one.

(Kiladis et al. 2005). The results are insensitive to reasonable variations in these filters, although neither filter captures the Kelvin–MJO hybrid systems that have periods of 20–30 days (Roundy 2012a,b). Tropical cyclones themselves produce large rainfall anomalies that can project onto filtered equatorial wave diagnostics (Schreck et al. 2011, 2012; Aiyyer et al. 2012). While the Kelvin and MJO bands are generally less susceptible to this contamination, the tropical cyclone anomalies are removed before filtering following Schreck et al. (2011).

b. *Binning methodology*

The relationship between the Kelvin waves and the tropical cyclones is identified by the time between the passage of the wave's maximum rainfall anomaly (crest) and the genesis. Figure 1 shows the rainfall variance that falls within the Kelvin band overlaid with the tropical cyclogenesis locations for 1998–2012. Kelvin waves are most active in the intertropical convergence zone (ITCZ; Kiladis et al. 2009). The waves are thus identified by averaging Kelvin-filtered rainfall from the equator to 10° latitude in either hemisphere (Fig. 1, green lines). Crests in the waves are defined to be local maxima in time at a given longitude that exceed 1.0 standard deviation at that longitude.

I matched these Kelvin wave crests with tropical cyclogenesis events. Only storms that formed with 20° latitude of the equator (Fig. 1, blue lines) were

TABLE 1. For each basin, the total number of storms during 1998–2013 and the average number of storms that form at each 1-day lag from −9.5 to +9.5 days. Also shown are the lags that produce the most and the fewest storms, the number of storms that form at that lag, and the ratio between them. Boldface values are significantly different from the mean.

			Max			Min			
Basin	Total storms	Bin avg	Lag (days)	Storms	% of avg	Lag (days)	Storms	% of avg	Ratio
North Atlantic	159	19.8	2.5	**29**	**146**	−1.5	13	66	2.2
Eastern Pacific	284	28.1	3.5	**40**	**142**	−2.5	19	68	2.1
Western Pacific	380	58.9	0.5	**71**	**121**	−0.5	42	71	1.7
North Indian	83	10.4	2.5	**19**	**183**	−7.5	5	48	3.8
South Indian	252	38.0	3.5	**51**	**134**	−1.5	26	68	2.0
South Pacific	137	21.0	1.5	**30**	**143**	−0.5	**11**	**52**	2.7

considered in each basin. Kelvin wave convection is generally confined to the ITCZ and the dynamical signals are strongest near the equator (Kiladis et al. 2009). Therefore, these waves presumably play a lesser role in higher-latitude storms. For each storm, I identified all Kelvin wave crests that occurred at the same longitude and on the same side of the equator as the cyclogenesis. I then binned the crests by 1-day lags relative to genesis (Fig. 2). The bins are defined such that the −1.5-day bin includes storms forming at −2.0, −1.75, −1.5, and −1.25 days. Similarly, the +1.5-day bin includes +1.0, +1.25, +1.5, and +1.75 days. Positive lags indicate that the wave crest led the genesis. A given storm could be binned with multiple lags, one for each crest that passed through its genesis longitude.

To confirm the Kelvin waves' influences on tropical cyclogenesis, I assessed the statistical significance of the

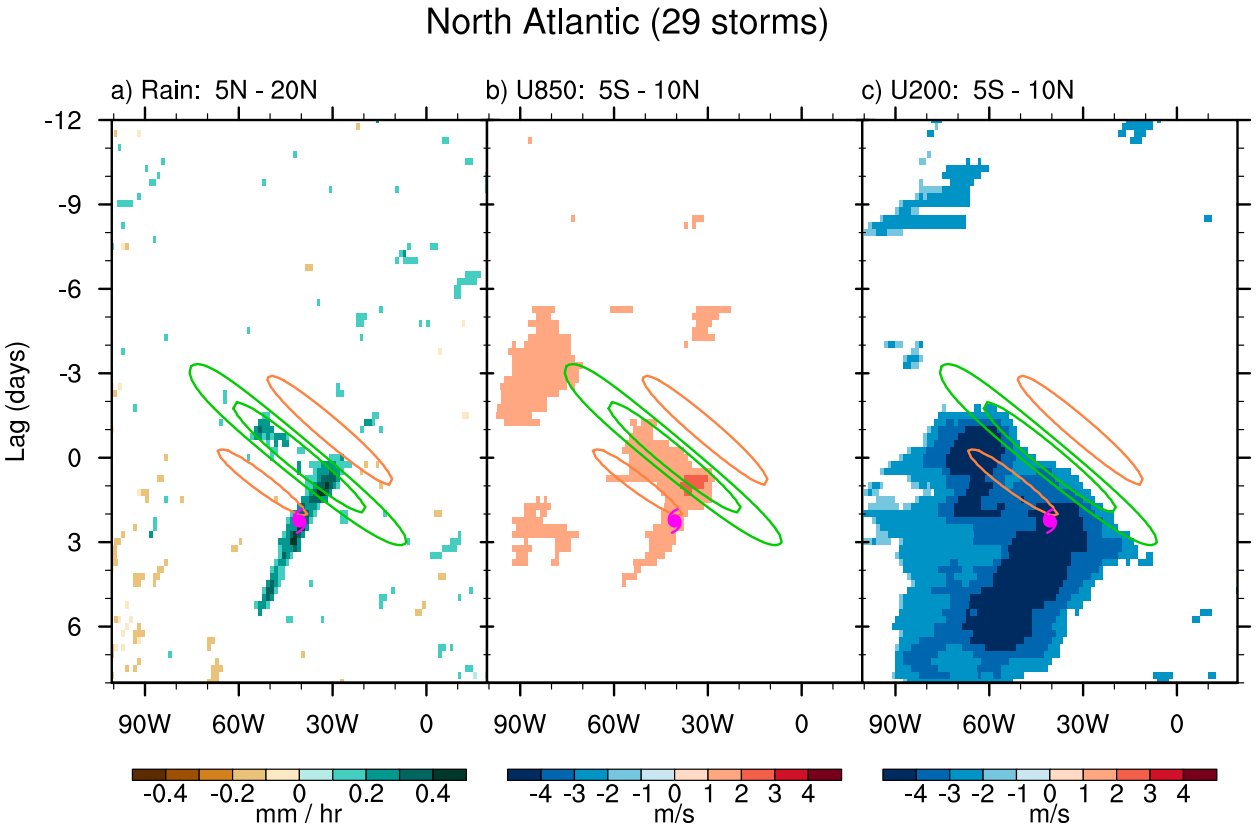

FIG. 3. Lag–longitude Hovmöller composite anomalies of (a) unfiltered rain rate averaged 5°–20°N, (b) 850-hPa zonal wind averaged 5°S–10°N, and (c) 200-hPa zonal wind averaged 5°S–10°N for the 29 storms that formed 2.5 days after a Kelvin wave crest in the North Atlantic. Kelvin-filtered rainfall anomalies averaged 0°–15°N are contoured every 0.05 mm h^{-1} with wet contours in green and dry in orange. Lag 0 corresponds to the Kelvin wave crest, and the median tropical cyclogenesis time is indicated by the hurricane symbol. Composite longitude is relative to the tropical cyclogenesis location. Longitude labels are for the median genesis longitude and are shown only for reference. Only those composite anomalies that are 95% significant are shown.

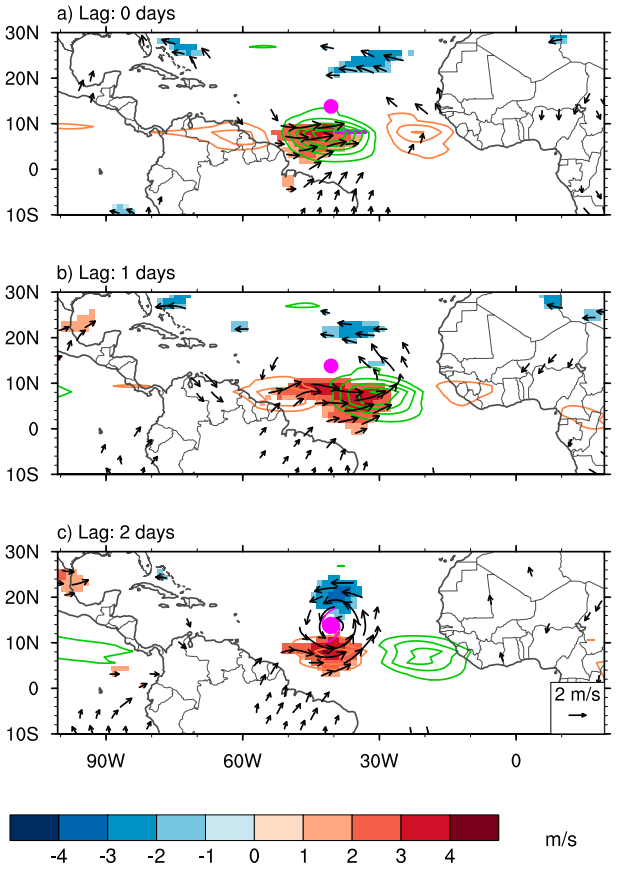

FIG. 4. Composite 850-hPa wind anomalies (vectors) with the zonal component shaded for the 29 storms that formed 2.5 days after a Kelvin wave crest. Kelvin-filtered rainfall anomalies are contoured every 0.05 mm h^{-1} with wet anomalies in green and dry in orange. Composites are relative to the tropical cyclogenesis longitude, indicated by the magenta dot. The geography and longitude labels are relative to the median genesis longitude and are for reference only. Only anomalies that are 95% significant are shown.

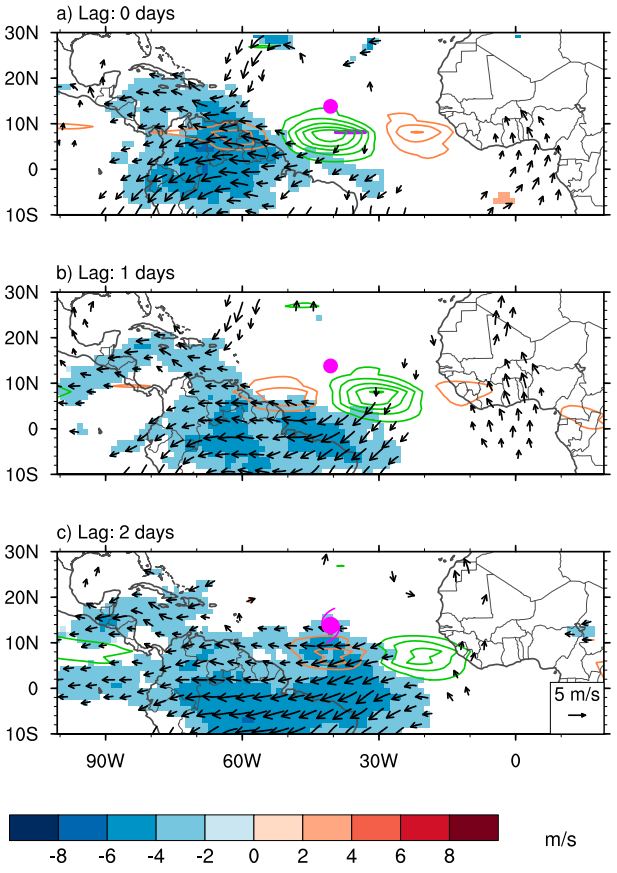

FIG. 5. As in Fig. 4, but for 200-hPa wind anomalies.

number of storms in each bin. The null hypothesis was that the number of storms in each bin would be the same if there were no wave influence. To test this hypothesis, I averaged the number of storms in each bin from −9.5 to +9.5 days (Fig. 2, solid lines). This average was considered the normal number of storms per lag, and the right axis in Fig. 2 shows the percentage deviations from that average.

I then used the cumulative density function of the binomial distribution to determine the 95% probability range of counts (Fig. 2, dashed lines). The binomial distribution determines the probability Pr of observing k events given the number of trials n and the probability p of observing the event on any given trial. In this case, the number of trials n is the sum of the number of storms in all the bins −9.5 to +9.5 days. The probability p that a storm will fall within any given bin is 1/20 (0.05), as there are 20 bins in the histogram and each storm has an equal probability of falling in any of them by the null hypothesis. I defined the cumulative probability Pr to be 0.025 and 0.975 to create a 95% range. These parameters are inserted into the cumulative distribution function to solve for $k_{2.5}$ and $k_{97.5}$. Counts within any bin that fall outside this range are considered statistically significant.

c. *Compositing methodology*

To assess how the Kelvin waves affected tropical cyclogenesis, I created composites for storms that developed within the most favorable lag for each basin. For comparison, the data in these composites were rotated such that the genesis longitudes aligned with the median genesis longitude for all storms in the composite. Similarly, the composites were aligned in time such that the Kelvin wave crest occurs at lag 0 at the genesis longitude.

Statistical significance of the composites is evaluated using a method similar to that in Schreck et al. (2013a,b). The null hypothesis is that the composite anomalies could have arisen from random variability. The hypothesis is tested by generating 10 000 null composites that each have the same sample size as the original storm composite as follows:

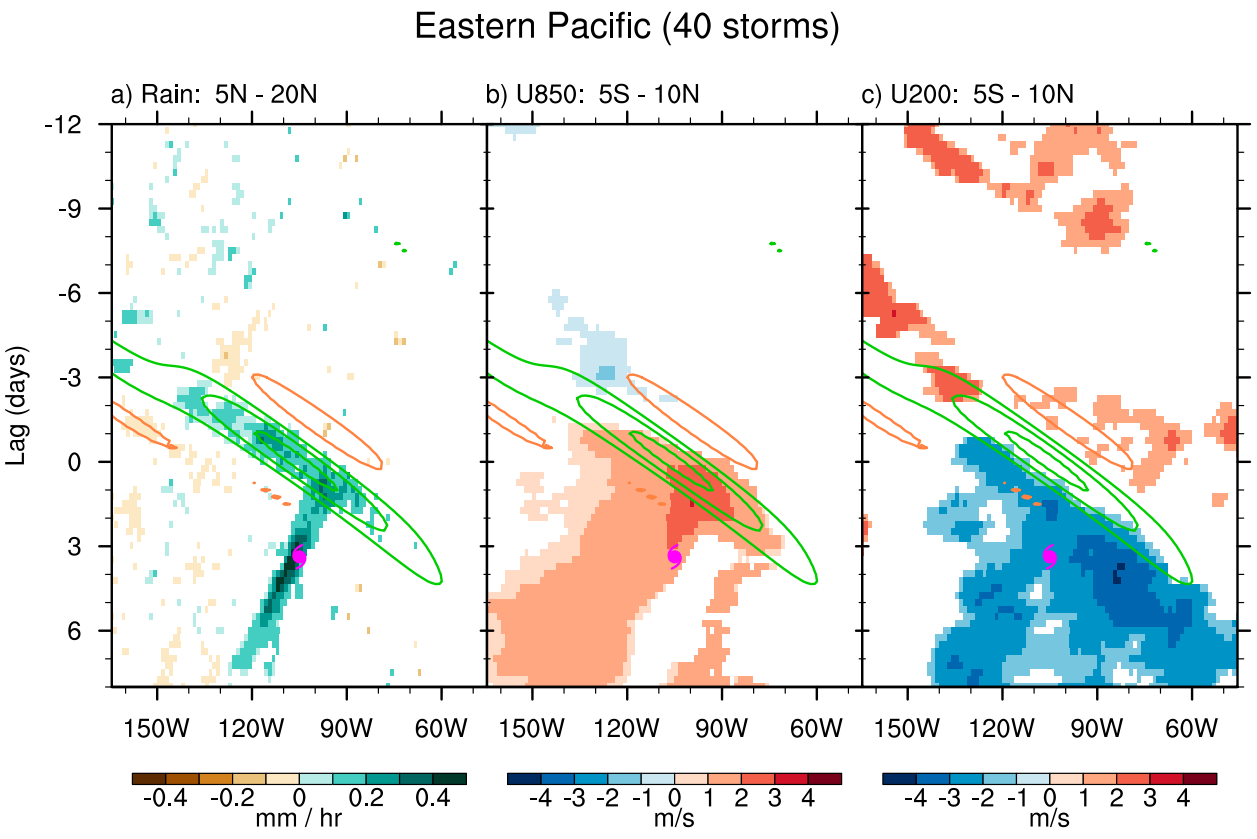

FIG. 6. As in Fig. 3, but for the 40 eastern Pacific storms that formed 3.5 days after a Kelvin wave crest.

1) Randomly select one of the composite storms with replacement. Use that storm's genesis month and day, but randomly select a different year from 1998 to 2013.
2) Randomly select another storm with replacement. Use this storm's genesis longitude.
3) Repeat the above steps to produce a synthetic sample of the same size as the original and generate a null composite.

Once the above process has been repeated for 10 000 null composites, these composites are compared with the original. At each data point, the original composite is considered statistically significant at the 95% level using a two-tailed test if it is either greater than or less than 9750 of the null composites.

3. Results

a. Modulation by lag from wave crest

Figure 2 shows the number of storms that formed on each day relative to the convective peak of a Kelvin wave in each basin, and Table 1 shows the days that have the most and the fewest storms. The results for the North Atlantic (Fig. 2a) are qualitatively similar to those of Ventrice et al. (2012a, see their Fig. 9), even though they defined the lag relative to the leading edge of the Kelvin wave convection rather than its peak. In both studies, cyclogenesis is suppressed before wave passage and enhanced afterward, particularly at a lag of +2 days. Ventrice et al. (2012a) found a modulation of about 4.5 times between the most and least active lags. The modulation in our study is only 2.2, perhaps because of differences in the periods used. I used all months during 1998–2013, whereas Ventrice et al. used June–September 1979–2009.

The numbers in Fig. 2 exhibit significant day-to-day variability. In the north Indian Ocean (Fig. 2d), for example, less than half as many storms form at a lag of +3.5 as did at the neighboring lags +2.5 and +4.5 days. In general, however, cyclogenesis is favored in the 3 days after the passage of a Kelvin wave and inhibited in the 3 days before. The patterns are most apparent in the North Atlantic, eastern Pacific, and south Indian basins (Figs. 2a,b,e), whereas they are less clear in the western Pacific, north Indian, and South Pacific basins (Figs. 2c,d,f). Every basin except for the western Pacific has a ratio of at least 2:1 between the most and least active lags (Table 1). All six basins have at least one lag with a statistically significant increase in genesis. The south Indian Ocean is the only basin with multiple lags that show significant increases (+2.5, +3.5,

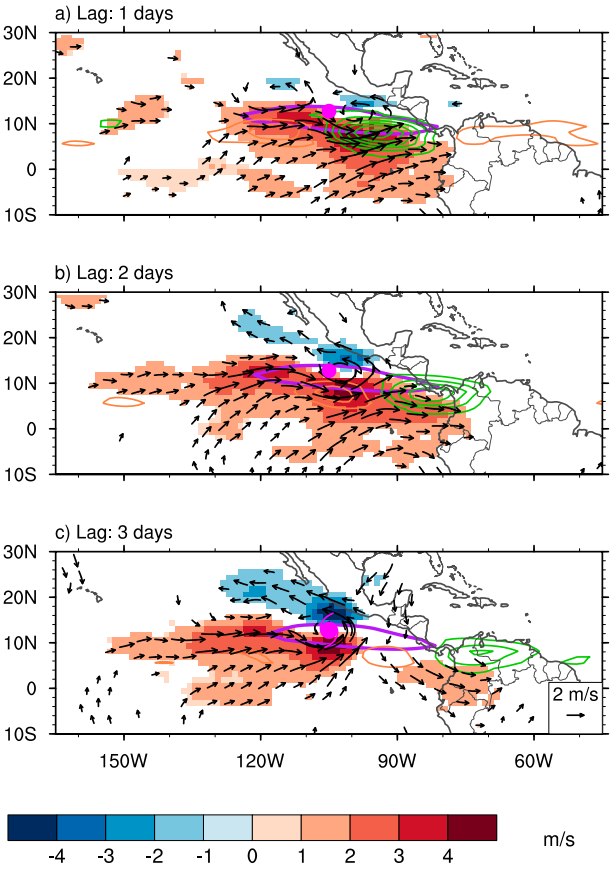

FIG. 7. As in Fig. 4, but for the 40 eastern Pacific storms that formed 3.5 days after a Kelvin wave crest. Thick purple contours identify MJO-filtered rainfall anomalies at 0.05 mm h^{-1}.

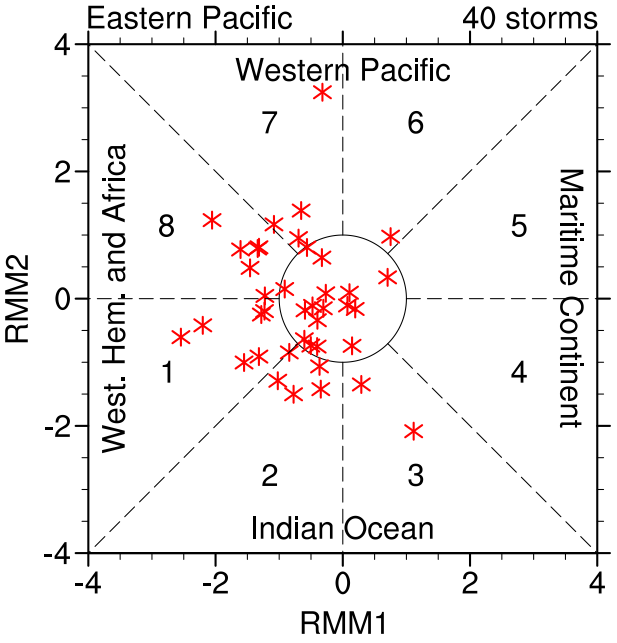

FIG. 8. RMM phases on the days of tropical cyclogenesis for the 40 eastern Pacific storms that formed 3.5 days after a Kelvin wave crest.

and +5.5 days) (Fig. 2e). The eastern Pacific is the only basin with a statistically significant decrease in genesis at any lag (−0.5 days) (Fig. 2b, Table 1).

The statistical significance test in Fig. 2 might be too liberal. The number of storms for any given lag has just a 5% chance of falling outside of the dashed lines by coincidence, which implies statistical significance. Given that each basin has 20 bins, however, the odds are 64% that any one out of those 20 would *appear* significant by random chance. If this effect had been accounted for (Šidák 1967; Wilks 2006), then none of the basins would have shown statistically significant results. In Fig. 2, however, *all* six basins have at least one lag with a significant increase, which only had a 6.9% (0.64^6) chance of occurring randomly. Furthermore, *every* basin has a statistically significant increase in genesis in one of the same three lags (0.5, 1.5, and 2.5 days), which would happen less than 0.001% of the time by chance. This similarity of the histograms between basins, combined with the physical connections between the Kelvin waves and tropical cyclogenesis that will be shown in the next section, provides confidence that Kelvin waves can in fact enhance tropical cyclogenesis.

b. *Mechanisms for modulation*

1) NORTH ATLANTIC

The most favorable lag in the North Atlantic is +2.5 days (Fig. 2a), during which 29 of the 159 storms formed. The storms forming at this lag were 46% above the average of all bins (Table 1). Figure 3 shows composite Hovmöllers of the storms forming at this lag. The strongest signal in the unfiltered rainfall anomalies (Fig. 3a, shading) is the westward propagation of the tropical cyclone itself and its pregenesis easterly wave. Eastward propagation with the Kelvin wave is more subtle but also visible. Because the tropical cyclone forms 2.5 days after the wave crest, it no longer benefits from the wave's enhanced convection. Interestingly, the storm actually develops within the convectively suppressed phase. Composites for midlevel humidity (not shown) showed similar patterns as the rainfall (Fig. 3a).

The 850-hPa zonal wind anomalies show a similar pattern to the rainfall with eastward propagation of westerly anomalies with the Kelvin wave (Fig. 3b). The Kelvin wave is more prominent at 200 hPa (Fig. 3c). Upper-level easterly anomalies spread eastward with the Kelvin wave's convection. They persist several days after the passage of the Kelvin wave and even through the suppressed phase of the waves. Kelvin

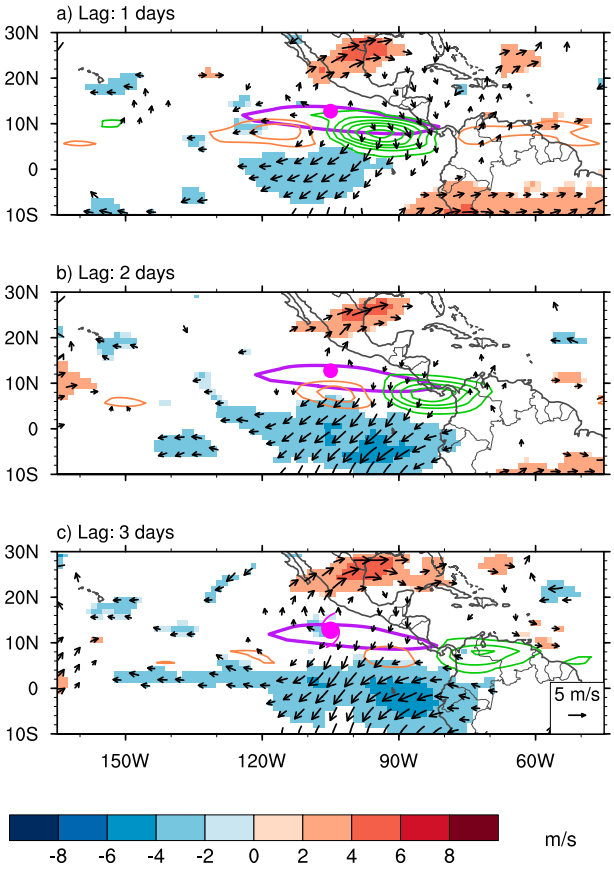

FIG. 9. As in Fig. 4, but for 200-hPa wind anomalies for the 40 eastern Pacific storms that formed 3.5 days after a Kelvin wave crest. Thick purple contours identify MJO-filtered rainfall anomalies at 0.05 mm h^{-1}.

wave composites from other studies (Wheeler et al. 2000; Straub and Kiladis 2002; Kiladis et al. 2009) generally produce anomalous 850-hPa easterlies and 200-hPa westerlies ahead of the convection. The lack of such anomalies in Fig. 3 and the persistence of the 200-hPa easterlies suggest the presence of a low-frequency background. Unlike previous studies, these composites are generated only for Kelvin waves that were associated with tropical cyclogenesis. As a result, they might be self-selected for periods, such as La Niña years, when conditions are already favorable for tropical cyclogenesis.

Figure 4 shows composite maps of the 850-hPa winds as the Kelvin wave leads to tropical cyclogenesis. Longitude in these composites is relative to the tropical cyclone, and the geography is shown only for reference relative to the median genesis longitude. The relationship between the Kelvin wave's convective envelope and the equatorial westerlies evolves as the tropical cyclone develops. At lag 0 days (Fig. 4a), the westerlies extend eastward to the leading edge of the Kelvin wave's convective envelope. The wind anomalies are predominately zonal at this time, and the overall structure is reminiscent of typical Kelvin wave composites (Straub and Kiladis 2003a; Kiladis et al. 2009). The westerlies extend farther eastward at lag +1 days (Fig. 4b), but the convection moves faster than the winds. As a result, the westerlies only reach the convective maximum of the wave. The eastern end of the westerlies also begins to curve into southerlies and even southeasterlies. The curvature is likely related to the intersection of the Kelvin wave and the pregenesis easterly wave. The winds become even more circular as the tropical cyclone forms at lag +2 days (Fig. 4c). The convective signal continues moving eastward and appears decoupled from the 850-hPa winds.

Figure 5 shows similar composite maps of the 200-hPa wind anomalies. Consistent with the Hovmöller composite (Fig. 3c), 200-hPa easterly anomalies spread eastward with the convective phase of the wave. The eastern end of these easterlies have a northerly component, consistent with outflow from the Kelvin wave's convection near 10°N. At higher latitudes (20°–30°N), the upper-level wind anomalies suggest extratropical wave breaking. Extratropical Rossby waves have a similar eastward phase speed as Kelvin waves. However, the strongest 200-hPa wind anomalies are near the equator, suggesting that these are driven primarily by Kelvin waves.

The 200-hPa easterlies extend from 10°S to 10°N (Fig. 5), about twice the meridional width of the 850-hPa westerlies (Fig. 4). The relationship between the Kelvin wave convection and the 200-hPa winds is also more consistent through the genesis process compared with the 850-hPa winds. Ventrice et al. (2012b) hypothesized that Kelvin waves play a role in modulating the vertical wind shear for tropical cyclogenesis. However, the 200-hPa anomalies are generally confined equatorward of the median genesis latitude (Fig. 5). Since the tropical cyclogenesis is most sensitive to the local vertical shear within 800 km of the storm center (DeMaria et al. 2005), the upper-level winds are more likely to be enhancing the upper-level outflow. The asymmetric nature of this enhancement can increase the angular momentum of the nascent storm (Molinari and Vollaro 1989).

2) EASTERN PACIFIC

The most favorable lag for the eastern Pacific was +3.5 days, which accounted for 50 of the 284 storms. Figure 6 shows the composite Hovmöllers for these tropical cyclones. The unfiltered rainfall anomalies associated with the Kelvin wave are much more apparent in the eastern Pacific (Fig. 6a) than they were in the

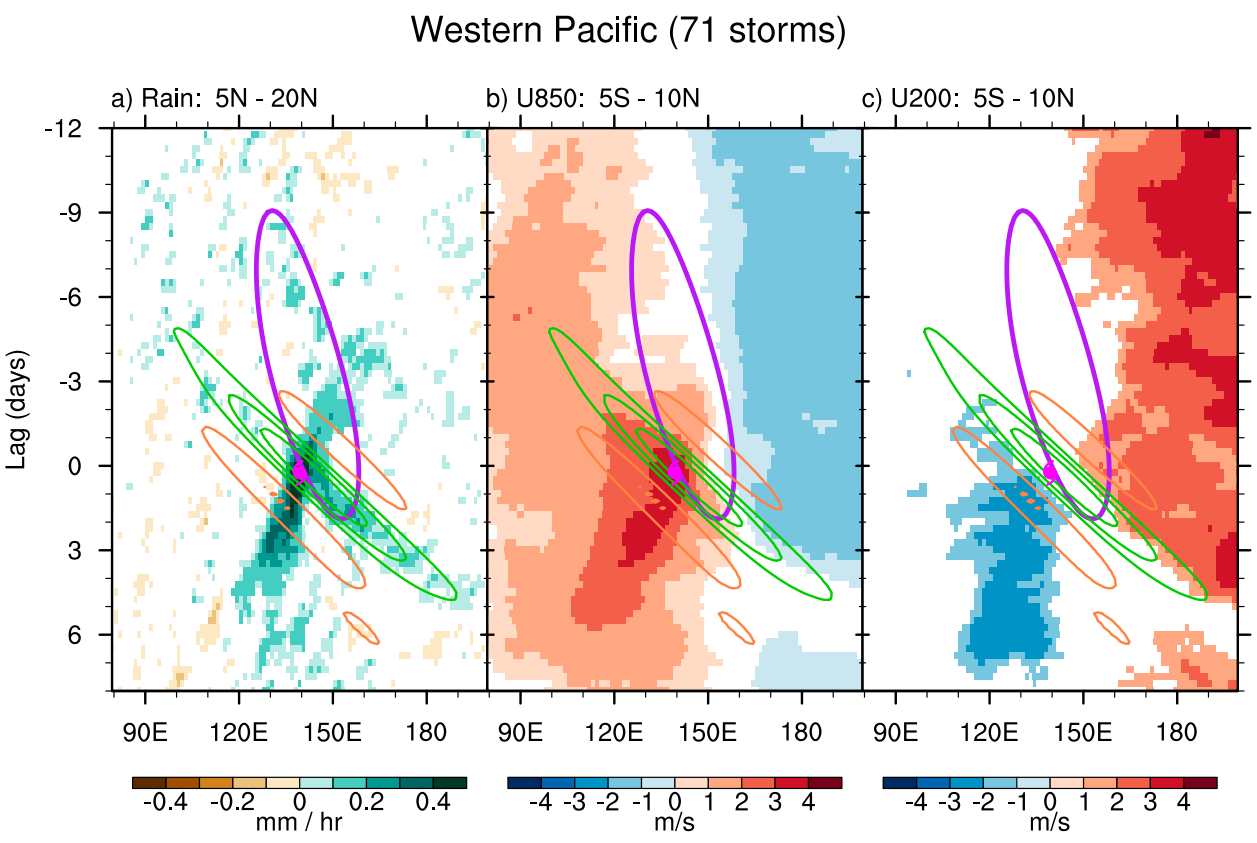

FIG. 10. As in Fig. 3, but for the 71 western Pacific storms that formed 0.5 days after a Kelvin wave crest. Thick purple contours identify MJO-filtered rainfall anomalies at 0.05 mm h^{-1}.

Atlantic (Fig. 3a). However, the 3.5-day lag between the wave crest and cyclogenesis means that the storm develops far removed from the Kelvin wave's convective envelope. As in the Atlantic, the nascent storms' rainfall can be traced backward through an easterly wave. The easterly wave signature only becomes apparent after the Kelvin wave passage, suggesting that the Kelvin wave significantly amplified the easterly wave.

The passage of the Kelvin wave in the eastern Pacific heralds the beginning of 850-hPa westerly anomalies and 200-hPa easterly anomalies. The anomalies at both levels persist longer than the period of the convective anomalies. A peak in the 850-hPa westerly anomalies propagates westward from the Kelvin wave crest associated with the pregenesis easterly wave. Westerly wind anomalies in the eastern Pacific can lead to easterly wave amplification and tropical cyclogenesis through barotropic energy conversion (Aiyyer and Molinari 2008; Rydbeck and Maloney 2014).

Figure 7 shows composite maps of the 850-hPa wind anomalies leading to genesis at lag +3.5 days. The westerly anomalies in the eastern Pacific (Fig. 7) are much broader in both zonal and meridional scale than in the North Atlantic (Fig. 4). At lag +1 days (Fig. 7a), the pregenesis easterly wave can be identified by the cyclonic circulation on the northeastern edge of the westerlies. This cyclonic curvature moves westward and intensifies as the easterly wave approaches tropical cyclogenesis (Figs. 7b,c).

Barotropic breakdown of the ITCZ is one pathway for cyclogenesis in the eastern Pacific (Nieto Ferreira and Schubert 1997). Westerly wind anomalies, such as those in Fig. 7, reduce the meridional gradient of absolute vorticity and make such breakdown more likely. The tropical cyclones form on the eastern periphery of the westerlies, consistent with modeling studies of ITCZ breakdown (Nieto Ferreira and Schubert 1997).

Figures 6 and 7 show the westerly anomalies in the eastern Pacific evolving in association with the Kelvin wave's convection. However, the spatial pattern in Fig. 7 is also reminiscent of the eastern Pacific's intraseasonal oscillation, which is related to the MJO (Rydbeck et al. 2013). The heavy purple contours in Fig. 7 indicate an enhancement of the ITCZ on the spatial and temporal

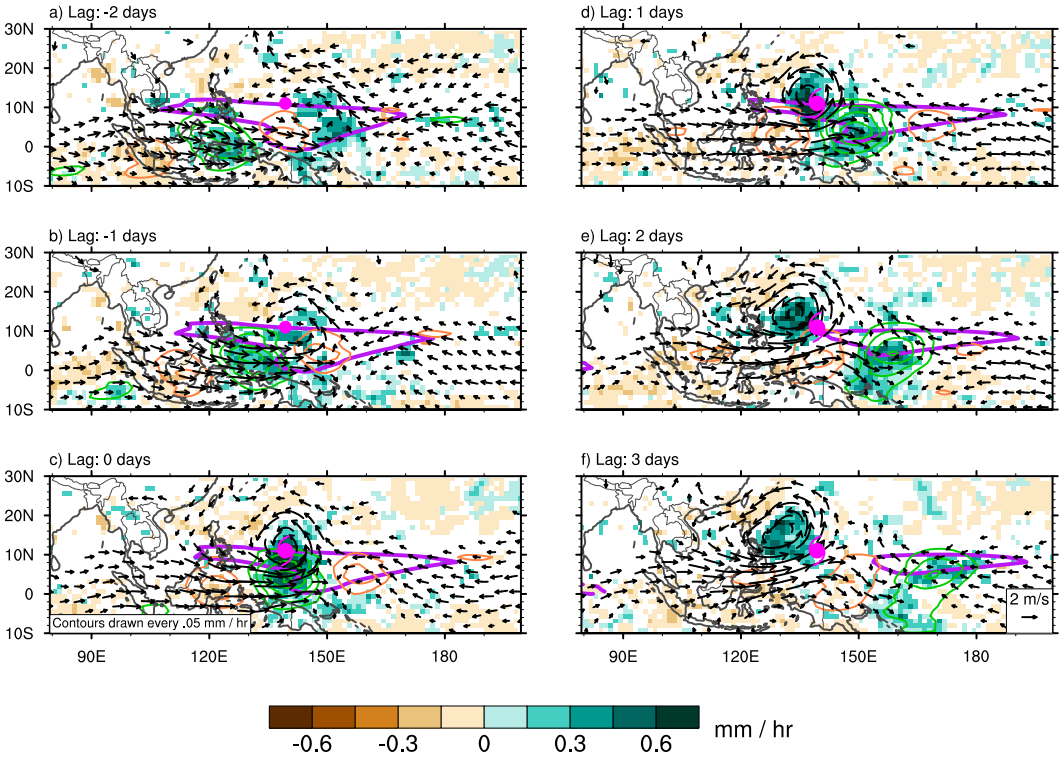

FIG. 11. As in Fig. 4, but for unfiltered rainfall anomalies (shaded) and 850-hPa wind anomalies (vectors) for the 71 western Pacific storms that formed 0.5 days after a Kelvin wave crest. Thick purple contours identify MJO-filtered rainfall anomalies at 0.05 mm h^{-1}.

scale of the MJO. Figure 8 shows the phase and amplitude of the Wheeler–Hendon (2004) Real-time Multivariate MJO (RMM) index on the genesis days for eastern Pacific storms that developed at lag +3.5 days. These storms are clustered toward phases 8/1, when the MJO enhances convection and low-level westerly anomalies in the eastern Pacific. The strongest Kelvin waves in the Western Hemisphere often emanate from the MJO's convection as it dissipates near the date line (Ventrice et al. 2012b; Sobel and Kim 2012), so the Kelvin wave modulation of tropical cyclones may be closely related to the MJO.

The 200-hPa winds associated with the Kelvin waves in the eastern Pacific (Fig. 9) are broadly similar to those in the Atlantic (Fig. 5). The easterly anomalies are generally confined to 10°S–10°N, well removed from the nascent tropical cyclone. They show a similar northeasterly curve, suggesting that these easterlies may enhance the outflow to encourage cyclogenesis.

3) WESTERN PACIFIC

The most favorable lag in the western Pacific was +0.5 days, the shortest of any basin (Fig. 2). However, it also had the smallest percentage increase in tropical cyclogenesis frequency, only 21% (Table 1). Figure 10 shows composite Hovmöllers for the 71 tropical cyclones that formed 0.5 days after a Kelvin wave crest. The rainfall composite (Fig. 10a) shows a clear Kelvin wave signature after the tropical cyclogenesis but not as much before. This is consistent with Sobel and Camargo (2005), who found evidence that tropical cyclones can actually initiate Kelvin waves. The 850-hPa zonal wind anomalies (Fig. 10b), however, show Kelvin-related westerly anomalies that trace backward several days before cyclogenesis.

The thick purple contour indicates that these storms typically form within a broader envelope of MJO-related convection (Fig. 10). Kelvin wave activity is even more closely tied with the MJO in the Eastern Hemisphere (Nakazawa 1988; Straub and Kiladis 2003b; Roundy 2012a). The leading edge of the MJO's convective envelope often resembles a Kelvin wave, and the strongest rainfall within that envelope is also associated with Kelvin waves (Schreck and Molinari 2011). In this case, the eastward-propagating 850-hPa westerly anomalies (Fig. 10b) are part of the MJO's transition from easterly anomalies to the east to westerly

anomalies, but they are punctuated by the surge in westerlies associated with the Kelvin wave. A similar interaction occurs at 200 hPa where the Kelvin wave initiates the MJO's easterly anomalies westward of 150°E (relative to median genesis longitude) and terminates the 200-hPa westerlies to the east.

Figure 11 shows composite maps of the rainfall and 850-hPa wind anomalies in the days before and after cyclogenesis. At lag −2 days (Fig. 11a), the low-level wind anomalies feed into the MJO's convection (thick purple contour) with broad easterlies over the central Pacific and westerlies extending from New Guinea to the Indian Ocean. The strongest westerly anomalies are associated with the convective Kelvin wave near 120°E, consistent with Fig. 10b. The Kelvin wave convection appears in the unfiltered rainfall from 5°S to 5°N. The Hovmöller (Fig. 10a) was averaged between 5° and 20°N to focus on the rainfall associated with genesis, which explains why the Kelvin signal was less apparent in there.

The pregenesis disturbance enhances the rainfall and cyclonically curved winds near 150°E at lag −2 days (Fig. 11a). Over the next two days (Figs. 11b,c) this disturbance converges with the Kelvin wave. Tropical cyclogenesis occurs at the point of maximum constructive interference between the disturbance and the Kelvin wave. Following genesis (Figs. 11d–f), the tropical cyclone moves northwestward. The hurricane symbol denotes where genesis occurred, not where the tropical cyclone is at any given time. The Kelvin wave's rainfall also continues propagating eastward after genesis. Associated with the wave, the easterly anomalies gradually give wave to westerlies.

The composite evolution in Figs. 10 and 11 resembles that observed in Schreck and Molinari's (2011) case study of Typhoons Rammasun and Chataan (2002). As in that case, the interaction of the Kelvin waves and the developing tropical cyclone occurs within the broadly favorable background of an MJO. Figure 12 shows the distribution of the RMM for the 71 storms used in the composites. These storms generally formed in phases 4/5/6, which would favor enhanced convection and tropical cyclogenesis in the western Pacific (Camargo et al. 2009; Klotzbach 2014). The composites in Figs. 10 and 11 show that the Kelvin waves further enhance this favorable environment to initiate cyclogenesis.

4) North and south Indian Ocean

The north Indian Ocean had the largest percentage increase (83%) for its most favorable lag (2.5 days) of any basin (Table 1). This large percentage occurs in part because the north Indian Ocean only had 83 tropical

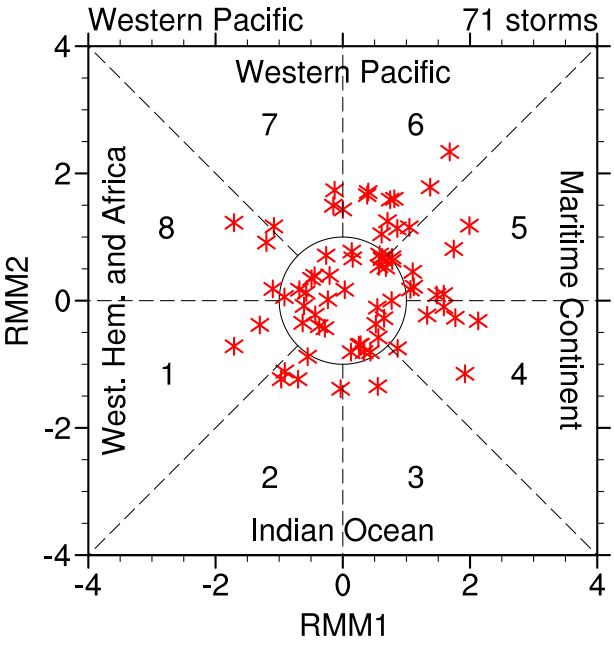

FIG. 12. As in Fig. 8, but for the 71 western Pacific storms that formed 0.5 days after a Kelvin wave crest.

cyclones from 1998 to 2013, the fewest of any basin. That explains why the reduction of storms in its least favorable lag (−7.5 days) was not statistically significant. Even though less than half as many storms formed at that lag, the low sample size makes this reduction more likely to have happened by random chance.

The composite Hovmöllers for the most favorable lags in the north and south Indian Ocean are shown in Figs. 13 and 14, respectively. As with the western Pacific (Fig. 10), these storms tend to be embedded with the convective phase of the MJO (thick purple contours). The Kelvin wave can be identified in the unfiltered rainfall anomalies in both basins (Figs. 13a and 14a). In the north Indian Ocean (Fig. 13a), the Kelvin wave is most apparent after its intersection with the pregenesis disturbance as in the western Pacific (Fig. 10a). Meanwhile, the south Indian Ocean shows a Kelvin wave signal tracing back to at least lag −2 days.

The 850-hPa zonal wind anomalies (Figs. 13b and 14b) also show a transition from easterlies to westerlies that moves eastward with the MJO's convective envelope. In both basins, the MJO's 850-hPa westerly wind anomalies surge eastward with the convective Kelvin wave. They weaken slightly following the Kelvin wave's suppressed phase, but otherwise persist through the end of the composite. No significant patterns are seen in the 200-hPa winds in the north Indian Ocean (Fig. 13c). The south Indian Ocean composite (Fig. 14c), on the other

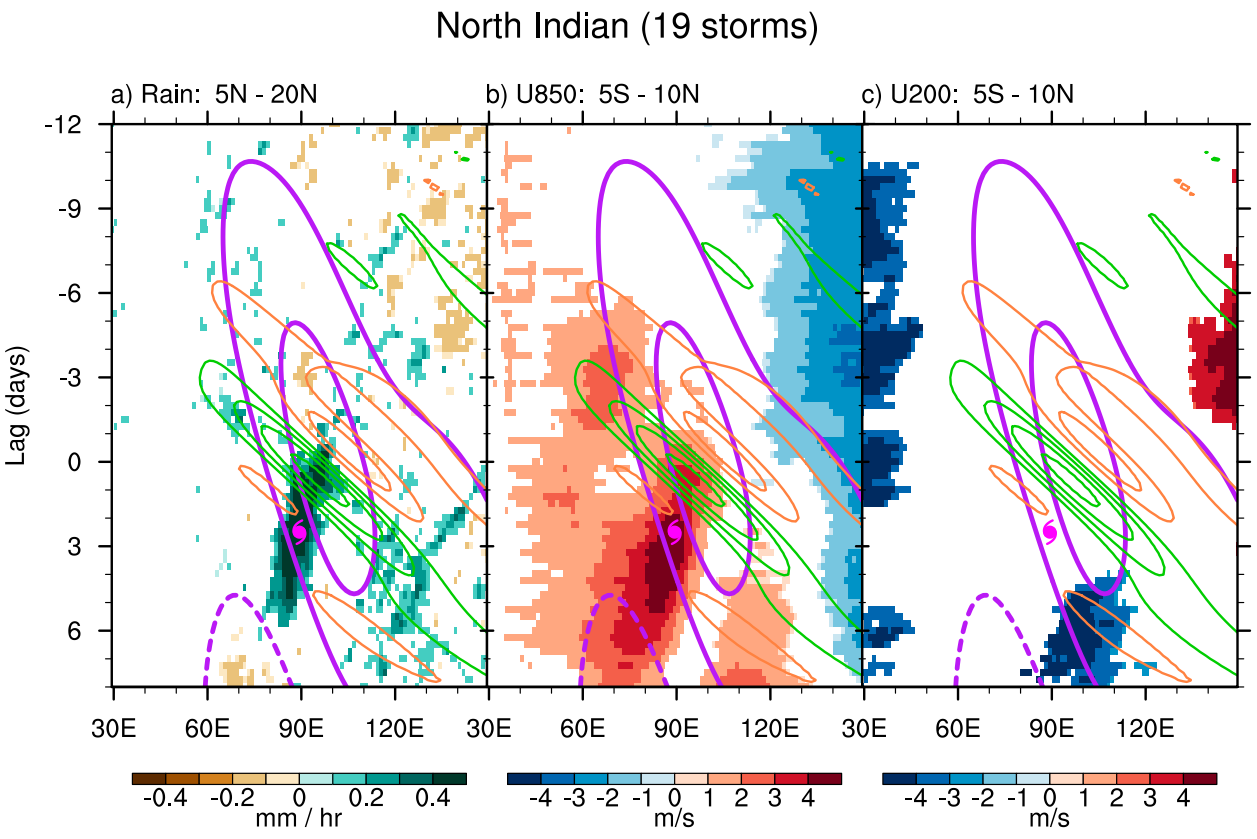

FIG. 13. As in Fig. 3, but for the 19 north Indian Ocean storms that formed 2.5 days after a Kelvin wave crest. Thick purple contours identify MJO-filtered rainfall anomalies at 0.05 mm h^{-1} with negative contours dashed.

hand, shows 200-hPa easterly anomalies that follow the Kelvin wave.

The composite tropical cyclone forms within an area of enhanced convection and westerly anomalies that moves westward at about 4 m s^{-1} in the north Indian Ocean and 2 m s^{-1} in the south Indian Ocean. These features initiate with the passage of the Kelvin wave crest at lag 0 days. However, their subsequent westward propagation creates a separation from the wave. In these cases, the Kelvin wave plays a more passive role in the cyclogenesis process. The Kelvin wave helps initiate the MJO's envelope of favorable conditions. The wave may also play a role in initiating the pregenesis disturbance. However, the interaction appears to end before cyclogenesis actually occurs.

5) SOUTH PACIFIC

The South Pacific was the only basin to have a statistically significant reduction in tropical cyclones at any lag. Only 11 storms formed at −0.5 days, compared with 30 at the most favorable lag, +1.5 days. The composite Hovmöllers (Fig. 15) shows the strongest intraseasonal signal in both the unfiltered rainfall (Fig. 15a) and 850-hPa zonal wind anomalies (Fig. 15b). While this signal roughly coincides with the MJO-filtered rainfall anomalies (thick purple contour), it moves slowly westward at about 2 m s^{-1}. The Kelvin wave is also apparent as a surge in these anomalies. In contrast to other basins, the Kelvin wave signals are firmly embedded within the intraseasonal envelope rather than at its leading edge. Tropical cyclogenesis occurs just 1.5 days after the intersection of the Kelvin wave with the intraseasonal signal. In this case, the wave enhances a favorable intraseasonal environment for cyclogenesis.

It is surprising that conditions do not appear significantly unfavorable for tropical cyclogenesis at lag −0.5 days, even though only 11 storms formed there. Rainfall would still have been enhanced and the equatorial westerlies would have already been in place. It is difficult to explain why 2.7 times more storms formed just two days later.

4. Conclusions

Tropical cyclogenesis is favored in the 3 days after the passage of a Kelvin wave and inhibited in the 3 days

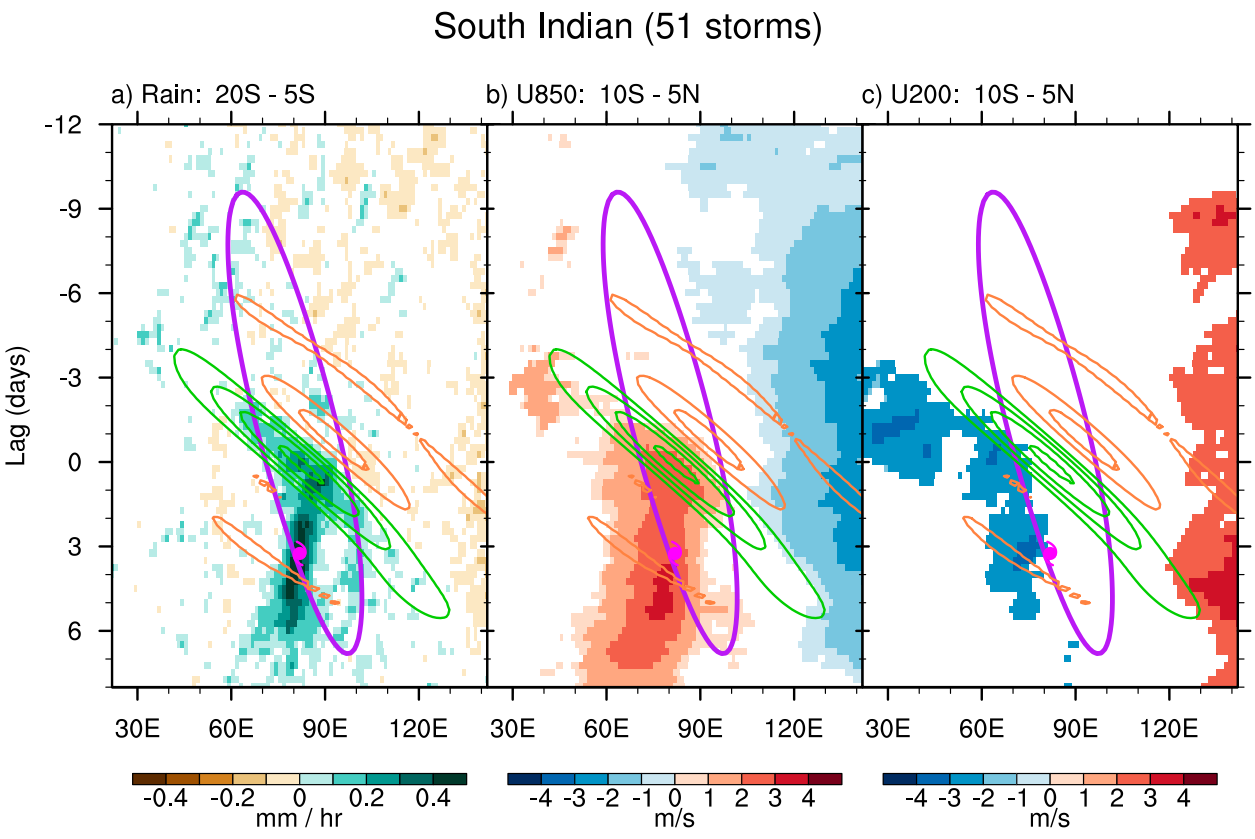

FIG. 14. As in Fig. 3, but for the 51 south Indian Ocean storms that formed 3.5 days after a Kelvin wave crest. Thick purple contours identify MJO-filtered rainfall anomalies at 0.05 mm h^{-1}.

before (Fig. 2, Table 1). The results broadly confirm the findings of Ventrice et al. (2012a,b) from the Atlantic and extends them to other basins. Composites of storms forming at the most favorable lags in each basin illustrate the dynamical effects of the waves on tropical cyclogenesis. These are summarized schematically in Fig. 16.

Because of the lag between the wave crest and the tropical cyclogenesis, the storms generally form within the dry phase of the Kelvin wave. This relationship suggests that the dynamical effects from the Kelvin wave likely outweigh its thermodynamic impacts. At 200 hPa, the Kelvin wave produces easterly anomalies to the south of the nascent tropical cyclone (Fig. 16a). Ventrice et al. (2012b) suggested that these easterly anomalies might modulate the background vertical shear. However, the composites in the current study show these anomalies to be too far removed from the storm to play a significant role. These upper-level winds have an equatorward meridional component that would act to enhance the outflow for the storm and thus enhance the storm's angular momentum (Molinari and Vollaro 1989).

At 850 hPa, the tropical cyclones generally form poleward of the Kelvin wave's equatorial westerly anomalies that provide enhanced cyclonic vorticity (Fig. 16b). These westerlies spread eastward with the propagation of the Kelvin wave's convection, but they persist longer than the wave's period. This persistence explains in part why the storms are able to form days after the Kelvin wave's convection has already moved away.

In addition to rainfall, 850-hPa winds, and 200-hPa winds, I also examined similar composites of the Kelvin waves and tropical cyclogenesis for other cyclogenesis factors like vertical shear, midlevel humidity, potential vorticity, velocity potential, and temperature (not shown). Vertical shear patterns were qualitatively similar to the 200-hPa winds, and midlevel humidity was strongly aligned with the rainfall anomalies. Linear shallow-water Kelvin waves cannot produce PV anomalies, but diabatic heating in observed convectively coupled Kelvin waves can (Roundy 2008; Ferguson et al. 2009; Dias and Pauluis 2009; Schreck and Molinari 2011). Unfortunately, the low-level potential vorticity composites (not shown) were dominated by smaller-scale features, so it was difficult to find coherent

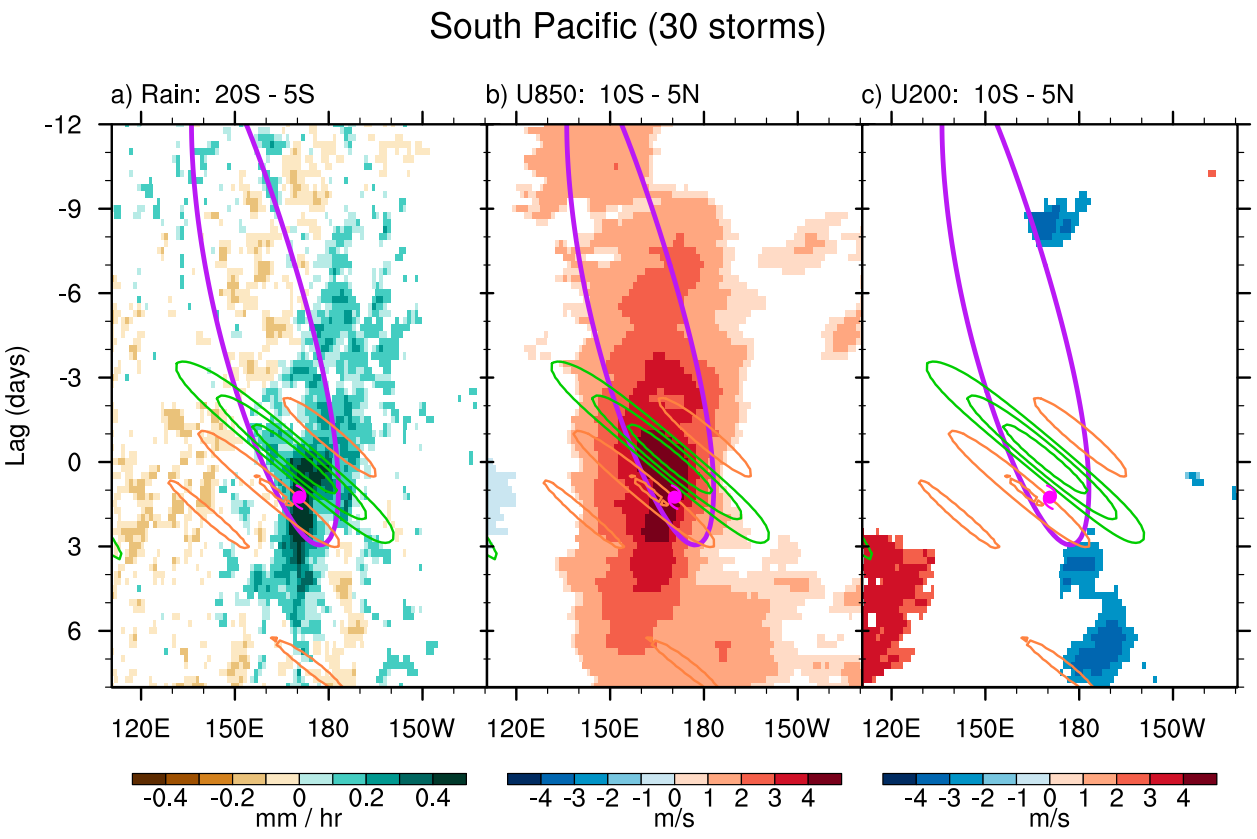

FIG. 15. As in Fig. 3, but for the 30 South Pacific storms that formed 1.5 days after a Kelvin wave crest. Thick purple contours identify MJO-filtered rainfall anomalies at 0.05 mm h^{-1}.

patterns. On the other hand, velocity potential and temperatures were largely driven by low-frequency signals like the MJO.

Figure 16c uses a Hovmöller schematic to place the evolution of the 850-hPa anomalies in the context of the MJO and the Kelvin waves. The composites show that the Kelvin waves are embedded within the MJO. The MJO produces a gradual transition from easterly to westerly anomalies. That transition is punctuated by an eastward surge in the westerly anomalies with the Kelvin wave, similar to that described by Schreck and Molinari (2011). It is difficult to separate the contributions of the Kelvin waves and the MJO, and their relative importance for cyclogenesis deserves further research. Based on the evolution of the westerlies in the current study, I hypothesize the Kelvin wave dictates the onset of the westerly anomalies and the MJO determines its duration.

The current study also reinforces that Kelvin waves are unlikely to initiate tropical cyclogenesis by themselves. Instead, they usually interact with an easterly wave (i.e., westward-moving pregenesis disturbance). This disturbance can be identified in composites of rainfall and 850-hPa zonal winds. It either originates or significantly amplifies around lag 0 days when it intersects with the Kelvin wave (Fig. 16c). Recent studies (Mekonnen et al. 2008; Ventrice et al. 2012a; Ventrice and Thorncroft 2013) have pointed similar interactions near Africa, but more research is needed into the interaction between Kelvin waves and easterly waves in other regions.

The intersection with the Kelvin wave's convection would enhance the easterly wave's own convection and vorticity. The westerly anomalies trailing the Kelvin wave could also have a favorable effect on the easterly wave. They could enhance the easterly waves through barotropic energy conversion (Aiyyer and Molinari 2008; Rydbeck and Maloney 2014). The Kelvin wave westerly anomalies could also help close the easterly wave's circulation, especially in the Lagrangian framework (Dunkerton et al. 2009). Since easterly waves and Kelvin waves are two of the most dominate modes of tropical synoptic variability, their interactions need to be better understood.

Acknowledgments. This study benefited from discussions with James Kossin, Philip Klotzbach, Michael

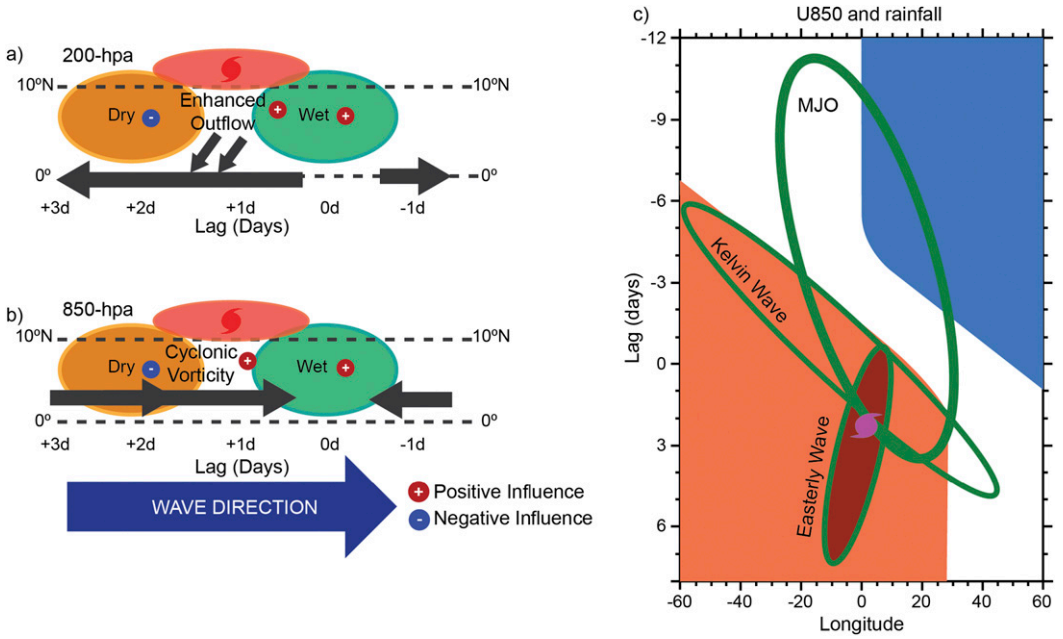

FIG. 16. Schematic summarizing the relationships between the Kelvin waves and tropical cyclogenesis observed in this study at (a) 200 and (b) 850 hPa. The horizontal axis is time in days from the wave crest, but it could also be viewed as longitude. The tropical cyclone generally forms outside of the wave's enhanced convection and moisture. Instead, it develops with enhanced (a) outflow at 200 hPa and (b) cyclonic vorticity, both of which persist on time scales longer than that of the wave. (c) Time–longitude Hovmöller schematic of 850-hPa zonal wind anomalies and rainfall anomalies associated with the Kelvin wave, the MJO, and the pregenesis easterly wave. The Kelvin wave is embedded within the MJO and affects the greatest change in the zonal wind anomalies. The easterly wave initiates or intensifies within the Kelvin wave and enhances the westerly anomalies until genesis occurs around 2.5 days after the interaction with the Kelvin wave crest.

Ventrice, and Eric Blake. It was supported through NASA PMM Grant NNX13AH47G. The schematic, Fig. 16, was prepared by Deborah Riddle. The NCAR Command Language (NCL) (UCAR/NCAR/CISL/VETS 2014) was used for all other analysis and plotting.

REFERENCES

Aiyyer, A., and J. Molinari, 2008: MJO and tropical cyclogenesis in the Gulf of Mexico and eastern Pacific: Case study and idealized numerical modeling. *J. Atmos. Sci.*, **65**, 2691–2704, doi:10.1175/2007JAS2348.1.

——, A. Mekonnen, and C. J. Schreck, 2012: Projection of tropical cyclones on wavenumber–frequency-filtered equatorial waves. *J. Climate*, **25**, 3653–3658, doi:10.1175/JCLI-D-11-00451.1.

Bessafi, M., and M. C. Wheeler, 2006: Modulation of South Indian Ocean tropical cyclones by the Madden–Julian oscillation and convectively coupled equatorial waves. *Mon. Wea. Rev.*, **134**, 638–656, doi:10.1175/MWR3087.1.

Camargo, S. J., M. C. Wheeler, and A. H. Sobel, 2009: Diagnosis of the MJO modulation of tropical cyclogenesis using an empirical index. *J. Atmos. Sci.*, **66**, 3061–3074, doi:10.1175/2009JAS3101.1.

DeMaria, M., M. Mainelli, L. K. Shay, J. A. Knaff, and J. Kaplan, 2005: Further improvements to the Statistical Hurricane Intensity Prediction Scheme (SHIPS). *Wea. Forecasting*, **20**, 531–543, doi:10.1175/WAF862.1.

Dias, J., and O. Pauluis, 2009: Convectively coupled waves propagating along an equatorial ITCZ. *J. Atmos. Sci.*, **66**, 2237–2255, doi:10.1175/2009JAS3020.1.

Dunkerton, T. J., M. T. Montgomery, and Z. Wang, 2009: Tropical cyclogenesis in a tropical wave critical layer: Easterly waves. *Atmos. Chem. Phys.*, **9**, 5587–5646, doi:10.5194/acp-9-5587-2009.

Ferguson, J., B. Khouider, and M. Namazi, 2009: Two-way interactions between equatorially-trapped waves and the barotropic flow. *Chin. Ann. Math.*, **30**, 539–568, doi:10.1007/s11401-009-0102-9.

Frank, W. M., and P. E. Roundy, 2006: The role of tropical waves in tropical cyclogenesis. *Mon. Wea. Rev.*, **134**, 2397–2417, doi:10.1175/MWR3204.1.

Huffman, G. J., and Coauthors, 2007: The TRMM Multisatellite Precipitation Analysis (TMPA): Quasi-global, multiyear, combined-sensor precipitation estimates at fine scales. *J. Hydrometeor.*, **8**, 38–55, doi:10.1175/JHM560.1.

Kiladis, G. N., K. H. Straub, and P. T. Haertel, 2005: Zonal and vertical structure of the Madden–Julian oscillation. *J. Atmos. Sci.*, **62**, 2790–2809, doi:10.1175/JAS3520.1.

——, M. C. Wheeler, P. T. Haertel, K. H. Straub, and P. E. Roundy, 2009: Convectively coupled equatorial waves. *Rev. Geophys.*, **47**, RG2003, doi:10.1029/2008RG000266.

Klotzbach, P. J., 2014: The Madden–Julian Oscillation's impacts on worldwide tropical cyclone activity. *J. Climate*, **27**, 2317–2330, doi:10.1175/JCLI-D-13-00483.1.

Knapp, K. R., M. C. Kruk, D. H. Levinson, H. J. Diamond, and C. J. Neumann, 2010: The International Best Track Archive for Climate Stewardship (IBTrACS). *Bull. Amer. Meteor. Soc.*, **91**, 363–376, doi:10.1175/2009BAMS2755.1.

Mekonnen, A., C. D. Thorncroft, A. R. Aiyyer, and G. N. Kiladis, 2008: Convectively coupled Kelvin waves over tropical Africa during the boreal summer: Structure and variability. *J. Climate*, **21**, 6649–6667, doi:10.1175/2008JCLI2008.1.

Molinari, J., and D. Vollaro, 1989: External influences on hurricane intensity. Part I: Outflow layer eddy angular momentum fluxes. *J. Atmos. Sci.*, **46**, 1093–1105, doi:10.1175/1520-0469(1989)046<1093:EIOHIP>2.0.CO;2.

Nakazawa, T., 1988: Tropical super clusters within intraseasonal variations over the western Pacific. *J. Meteor. Soc. Japan*, **66**, 823–839.

Nieto Ferreira, R., and W. H. Schubert, 1997: Barotropic aspects of ITCZ breakdown. *J. Atmos. Sci.*, **54**, 261–285, doi:10.1175/1520-0469(1997)054<0261:BAOIB>2.0.CO;2.

Rienecker, M. M., and Coauthors, 2011: MERRA: NASA's Modern-Era Retrospective Analysis for Research and Applications. *J. Climate*, **24**, 3624–3648, doi:10.1175/JCLI-D-11-00015.1.

Roundy, P. E., 2008: Analysis of convectively coupled Kelvin waves in the Indian Ocean MJO. *J. Atmos. Sci.*, **65**, 1342–1359, doi:10.1175/2007JAS2345.1.

——, 2012a: The spectrum of convectively coupled Kelvin waves and the Madden–Julian oscillation in regions of low-level easterly and westerly background flow. *J. Atmos. Sci.*, **69**, 2107–2111, doi:10.1175/JAS-D-12-060.1.

——, 2012b: Observed structure of convectively coupled waves as a function of equivalent depth: Kelvin waves and the Madden–Julian oscillation. *J. Atmos. Sci.*, **69**, 2097–2106, doi:10.1175/JAS-D-12-03.1.

——, and W. M. Frank, 2004: A climatology of waves in the equatorial region. *J. Atmos. Sci.*, **61**, 2105–2132, doi:10.1175/1520-0469(2004)061<2105:ACOWIT>2.0.CO;2.

Rydbeck, A. V., and E. D. Maloney, 2014: Energetics of east Pacific easterly waves during intraseasonal events. *J. Climate*, **27**, 7603–7621, doi:10.1175/JCLI-D-14-00211.1.

——, ——, S.-P. Xie, J. Hafner, and J. Shaman, 2013: Remote forcing versus local feedback of east Pacific intraseasonal variability during boreal summer. *J. Climate*, **26**, 3575–3596, doi:10.1175/JCLI-D-12-00499.1.

Schreck, C. J., and J. Molinari, 2011: Tropical cyclogenesis associated with Kelvin waves and the Madden–Julian oscillation. *Mon. Wea. Rev.*, **139**, 2723–2734, doi:10.1175/MWR-D-10-05060.1.

——, ——, and K. I. Mohr, 2011: Attributing tropical cyclogenesis to equatorial waves in the western North Pacific. *J. Atmos. Sci.*, **68**, 195–209, doi:10.1175/2010JAS3396.1.

——, ——, and A. Aiyyer, 2012: A global view of equatorial waves and tropical cyclogenesis. *Mon. Wea. Rev.*, **140**, 774–788, doi:10.1175/MWR-D-11-00110.1.

——, J. M. Cordeira, and D. Margolin, 2013a: Which MJO events affect North American temperatures? *Mon. Wea. Rev.*, **141**, 3840–3850, doi:10.1175/MWR-D-13-00118.1.

——, L. Shi, J. P. Kossin, and J. J. Bates, 2013b: Identifying the MJO, equatorial waves, and their impacts using 32 years of HIRS upper-tropospheric water vapor. *J. Climate*, **26**, 1418–1431, doi:10.1175/JCLI-D-12-00034.1.

——, K. R. Knapp, and J. P. Kossin, 2014: The impact of best track discrepancies on global tropical cyclone climatologies using IBTrACS. *Mon. Wea. Rev.*, **142**, 3881–3899, doi:10.1175/MWR-D-14-00021.1.

Šidák, Z., 1967: Rectangular confidence regions for the means of multivariate normal distributions. *J. Amer. Stat. Assoc.*, **62**, 626–633.

Sobel, A. H., and S. J. Camargo, 2005: Influence of western North Pacific tropical cyclones on their large-scale environment. *J. Atmos. Sci.*, **62**, 3396–3407, doi:10.1175/JAS3539.1.

——, and D. Kim, 2012: The MJO-Kelvin wave transition. *Geophys. Res. Lett.*, **39**, L20808, doi:10.1029/2012GL053380.

Straub, K. H., and G. N. Kiladis, 2002: Observations of a convectively coupled Kelvin wave in the eastern Pacific ITCZ. *J. Atmos. Sci.*, **59**, 30–53, doi:10.1175/1520-0469(2002)059<0030:OOACCK>2.0.CO;2.

——, and ——, 2003a: The observed structure of convectively coupled Kelvin waves: Comparison with simple models of coupled wave instability. *J. Atmos. Sci.*, **60**, 1655–1668, doi:10.1175/1520-0469(2003)060<1655:TOSOCC>2.0.CO;2.

——, and ——, 2003b: Interactions between the boreal summer intraseasonal oscillation and higher-frequency tropical wave activity. *Mon. Wea. Rev.*, **131**, 945–960, doi:10.1175/1520-0493(2003)131<0945:IBTBSI>2.0.CO;2.

Takayabu, Y. N., and M. Murakami, 1991: The structure of super cloud clusters observed in 1–20 June 1986 and their relationship to easterly waves. *J. Meteor. Soc. Japan*, **69**, 105–125.

UCAR/NCAR/CISL/VETS, 2014: The NCAR Command Language (version 6.2.1). NCAR, Boulder, CO, doi:10.5065/D6WD3XH5.

Ventrice, M. J., and C. D. Thorncroft, 2013: The role of convectively coupled atmospheric Kelvin waves on African easterly wave activity. *Mon. Wea. Rev.*, **141**, 1910–1924, doi:10.1175/MWR-D-12-00147.1.

——, ——, and M. A. Janiga, 2012a: Atlantic tropical cyclogenesis: A three-way interaction between an African easterly wave, diurnally varying convection, and a convectively coupled atmospheric Kelvin wave. *Mon. Wea. Rev.*, **140**, 1108–1124, doi:10.1175/MWR-D-11-00122.1.

——, ——, and C. J. Schreck, 2012b: Impacts of convectively coupled Kelvin waves on environmental conditions for Atlantic tropical cyclogenesis. *Mon. Wea. Rev.*, **140**, 2198–2214, doi:10.1175/MWR-D-11-00305.1.

Wheeler, M., and G. N. Kiladis, 1999: Convectively coupled equatorial waves: Analysis of clouds and temperature in the wavenumber–frequency domain. *J. Atmos. Sci.*, **56**, 374–399, doi:10.1175/1520-0469(1999)056<0374:CCEWAO>2.0.CO;2.

——, and H. H. Hendon, 2004: An all-season real-time multivariate MJO index: Development of an index for monitoring and prediction. *Mon. Wea. Rev.*, **132**, 1917–1932, doi:10.1175/1520-0493(2004)132<1917:AARMMI>2.0.CO;2.

——, G. N. Kiladis, and P. J. Webster, 2000: Large-scale dynamical fields associated with convectively coupled equatorial waves. *J. Atmos. Sci.*, **57**, 613–640, doi:10.1175/1520-0469(2000)057<0613:LSDFAW>2.0.CO;2.

Wilks, D. S., 2006: *Statistical Methods in the Atmospheric Sciences.* 2nd ed. Academic Press, 627 pp.